Experimental Simulation of Enhanced Geothermal Reservoir Stimulation

Lianbo Hu[1], Ahmad Ghassemi[1], John Pritchett[2], and Sabodh Garg[2]

[1]Reservoir Geomechanics and Seismicity Research Group,
The University of Oklahoma, Norman OK, USA
[2]Leidos Inc, San Diego, CA, USA

Keywords
Enhanced geothermal system, laboratory scale, self-potential, acoustic emission, hydraulic fracturing, circulation, tracers

ABSTRACT

Geothermal energy production by water circulation in natural and/or man-made fracture systems is referred to as enhanced or engineered geothermal systems (EGS). The permeable zones of an EGS must be created by stimulation, a process which involves fracture initiation and/or activation and propagation of discontinuities such as joints by pore pressure and stress perturbations. Economic design and operation of EGS can be achieved by reliable characterization of the stimulation results which relies mostly on analysis of micro-earthquake (MEQ) and tracers. In this work we study the reservoir stimulation process on a laboratory scale to improve the current understanding and to help quantify the fracture geometry using acoustic emission (AE) cloud, spontaneous potential (SP), and tracer analysis. To do so, we have developed a new poly-axial hydraulic fracturing test system which allows us to perform reservoir stimulation experiments on rock blocks with size up to 18' x18" x 18" under pore pressure and representative in-situ stress regimes while simultaneously recording SP and AE during fracturing and circulation. In this paper, we describe preliminary experiments conducted at room and elevated temperatures along with a circulation phase in the latter case. Reservoir stimulation has been accompanied by AE events that are generally correlated with the stress state and fracture geometry, however with less than expected intensity. Results show excellent correlation between the fracturing events and the SP signal.

1. Introduction

Geothermal energy is considered as a promising option for future clean and sustainable energy supply. However, certain technical barriers need to be removed for large scale utilization of the resources. Particularly, questions related to reservoir creation in different rock types and stress conditions need be addressed. Laboratory scale studies present a good opportunity to help resolve some of the pending challenges along with recent field-scale efforts within the framework of the FORGE (Frontier Observatory for Research in Geothermal Energy) initiative. The main purpose of this project is to gain a better understanding of the geometry and the heat exchange properties of the hydraulically induced fractures in enhanced or engineered geothermal systems (EGS). To realize this goal, a new lab-scale hydraulic fracture test system has been developed that allows us to replicate aspects of the EGS hydraulic fracturing treatment in the field. Our work improves the state-of-the-art by allowing the simultaneous monitoring of acoustic emission (AE), spontaneous potential (SP) and tracers during the stimulation and circulation phases.

2. The Lab-Scale EGS Test System

The developed lab-scale EGS system has several integrated subsystems. The main subsystems are: a polyaxial frame and heaters, hydraulic fracturing and circulation system, AE and SP acquisition system, and fluids and tracers. Figure. 1

Figure 1. Fully assembled test systems (left) and heating by circulating hot water (right).

(left) shows the fully assembled test systems and Figure. 1 (right) shows the heating by circulating hot water. More information about these subsystems are described in Hu (2016). At the flowing section, one preliminary test will be described and some preliminary interpretation will be provided and discussed. The hydraulic fracturing portion was tested at room temperature while the circulation portion was conduction at elevated temperature condition.

3. Laboratory Test

3.1 Test Setup

A 13 inch cubical Sierra White granite block was instrumented with AE and SP sensors and placed in the frame to verify the proposed test methodology and expose as many potential issues as possible. Figure. 2 (left) is a top view showing the layout of the wells and the AE sensors on the top surface, and Figure. 2 (right) is a longitudinal sectional view of the sample showing the interior layout of the wells. The injection hole was drilled with a 0.75 inch diameter drill bit. The drilled injection well has a depth of 7.5 inches and a diameter of 0.78 inch. High strength epoxy was poured into the hole to seal the annulus between the injection tubing and the wellbore wall leaving a 2.0 inch unsealed injection interval at the bottom. Four production wells with a depth of 9 inch were drilled 3.5 inches away from the injection well and have 5 inch unsealed production intervals at the bottom. The diameter of the production wells is 0.4 inch. A thermistor was put at the center of each unsealed intervals in the wells to measure the temperature. An SP sensor was placed in the injection well as a reference electrode. The SP sensors were made by soldering a coaxial cable to a thin circular copper sheet with a diameter of around 0.5 inch. Small alundum (aluminum oxide) balls were located inside the wells to occupy space in an effort to minimize the effect of wellbore storage. The locations of SP sensors and AE sensors are shown in Figure. 3. After the sample was put into the frame and the frame was fully assembled, a vacuum pump was connected to the frame to get as much air out of the frame as possible. Then, the sample was saturated and the principal stresses were applied

Table 1. Experimental parameters for the second Sierra White granite block.

p_p, psi	σ_v, psi	σ_h, psi	σ_H, psi
300	500	1000	1500

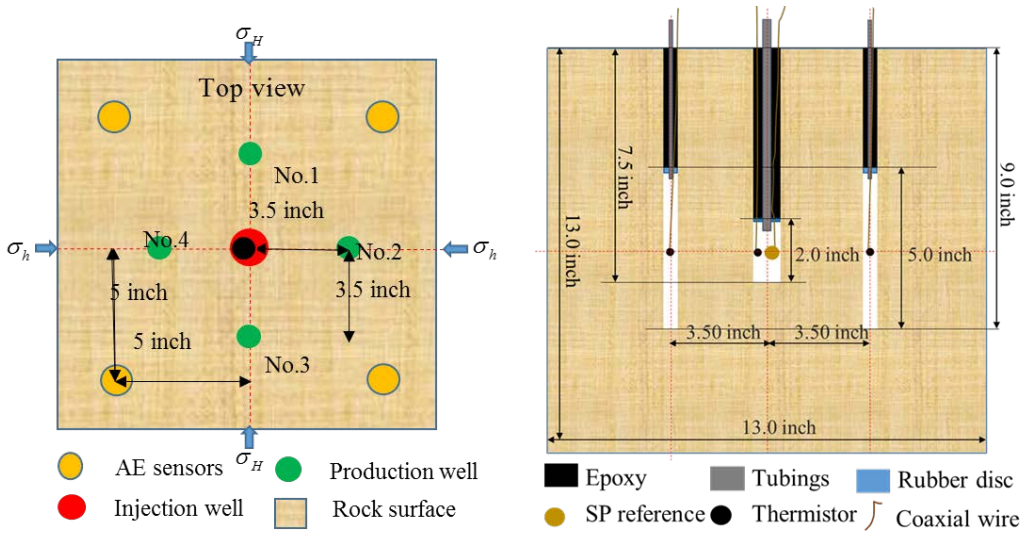

Figure 2. Layout of injection well and production wells with sensors.

by injecting oil into the flatjacks to pressurize them to a predetermined level. The space between the rock block and the inner surface of the loading frame is occupied by flatjacks, PEEK plates and steel plate spacers. Since we tried to control the induced fracture within the rock block, the hydraulic fracturing process was conducted carefully and controlled by a LABVIEW program. And it ended up with two hydraulic fracturing cycles. The test conditions and result are discussed below. Before the test, the rock sample was saturated with 0.002mol/L NaCl solution. The resulting solution was used for fracturing. The circulation fluid was got by adding tracer (Butanol) in the resulting fluid. The boundary condition for both these two fracturing test were the same and is list in Table 1.

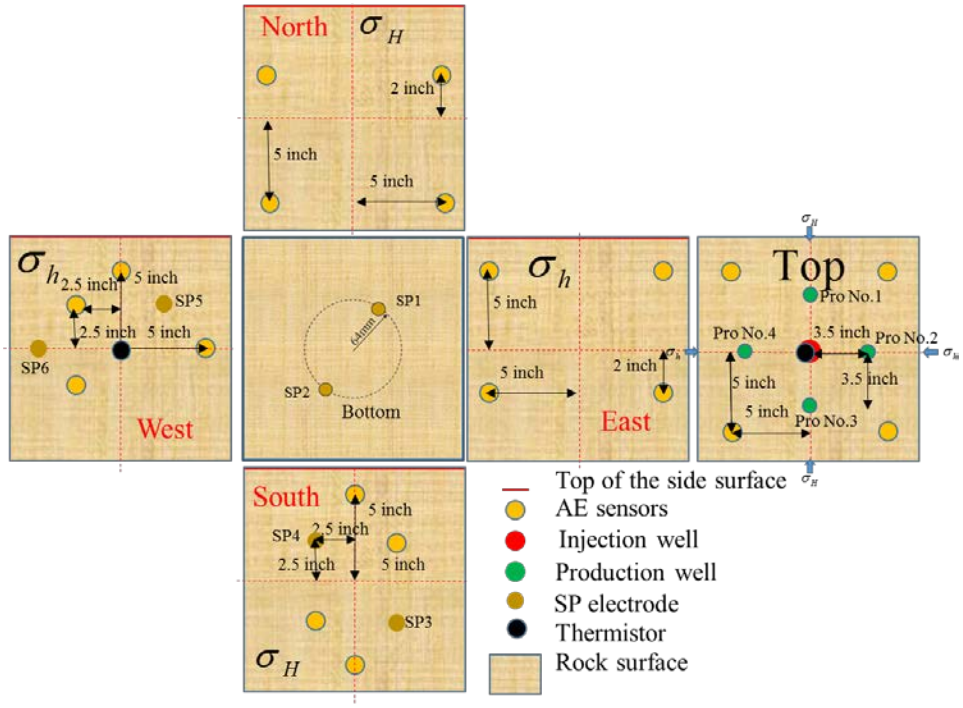

Figure 3. Fold-out diagram of the Sierra White block with AE sensors and SP sensors.

3.2 Permeability Measurement Before Fracturing Test

Before hydraulic fracturing the block, permeability measurement was conducted on the block by injecting resulting solution into the injection well at a constant pressure while all the production wells were shut-in. The boundary condition is list in Table 1. Considering that the open interval of the injection well is short compared to the size of the rock, spherical flow is assumed. Then, under stable flow the permeability can be determined from Eq.3:

$$k = \frac{Q_r \mu \left(1/R_w - 1/R_e \right)}{4\pi \left(P_e - P_w \right)} \tag{1}$$

where k is the rock permeability Q_r is volumetric flow rate, R_w and R_e are the equivalent radius of the injection interval and the rock block, respectively, P_e and P_w are the pore pressure at the boundary and the injection well.

Figure 4 shows the relative data with 500 psi injection pressure. The injection rate was obtained by fitting the fluid volume in the pump with a linear function. In this case, the injection rate is 0.000306ml/s. Then, Eq. 1, the block permeability was determined to be 546nD and 1150nD at the injection pressure of 500 psi and 650 psi, respectively.

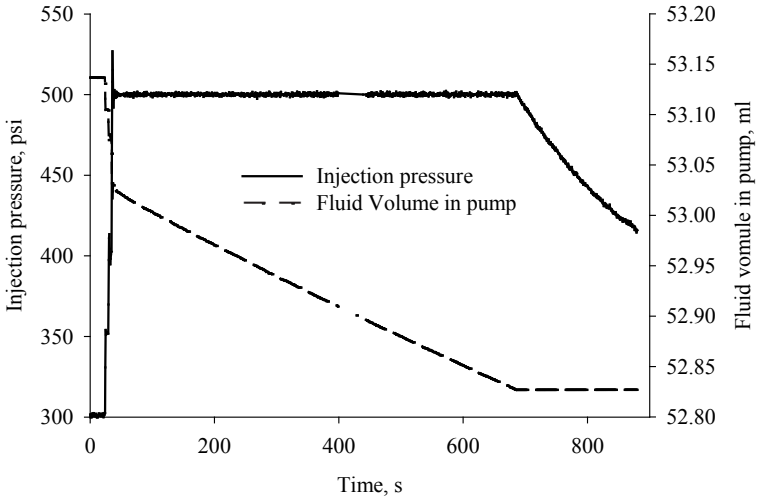

Figure 4. Permeability measurement test with injection pressure of 500 psi.

3.3 Test Parameters and Results of the First Cycle of Fracturing Test

As shown in Figure. 5, the injection rate was set to 0.5 ml/min at the beginning and then was increased to 1.0 ml/min after the injection pressure became stable. The test results show a good correlation between the injection pressure and the SP response. The breakdown pressure was 2938 psi which is 40% higher than the theoretical value

(2099psi) calculated from Hubbert and Willis model (Eq.2). The wellbore size effect and the rock heterogeneity could be the main reasons for this phenomenon. The tensile strength of Sierra White granite was measured to be 1549 psi from the Brazilian test (more Brazilian tests were conducted after the appearance of Hu 2016).

$$p_b = 3\sigma_h - \sigma_H - p_p + T \tag{2}$$

where $p_b, p_p, \sigma_h, \sigma_H, T$ are breakdown pressure, pore pressure, minimum horizontal principal stress, maximum horizontal principal stress and tensile strength of the rock, respectively.

Right after breakdown, the injection rate was reduced by 99 percent and then after 90 seconds, the injection was resumed. After 146.5 seconds of injection, the pump was shut. From the test result, it is clear that the injection pressure and the SP response are in good correspondence with each other. Also, it can be seen that the proportionality factor between SP and pressure is different before and after fracturing.

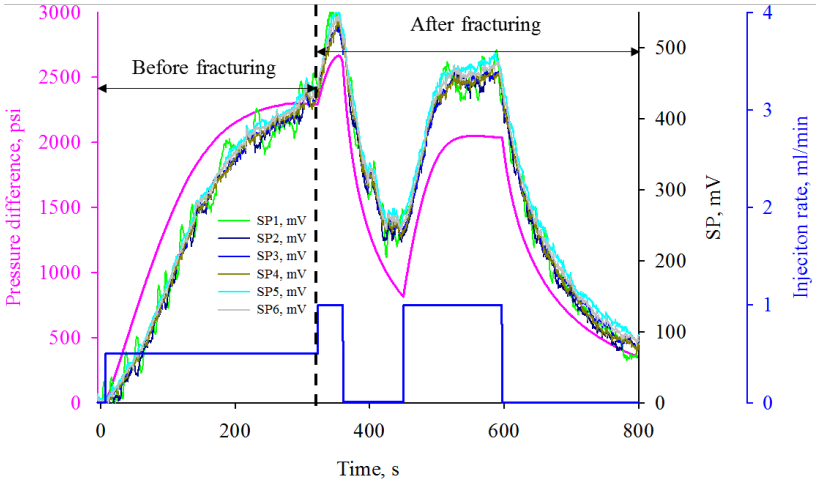

Figure 5. The recording data for second Sierra White granite block test (first cycle).

To provide a better understanding of the relationship between the pressure drop (pressure difference between the locations of the reference sensor (the injection well) and the SP signal sensors, and the SP recording (the potential difference between the SP sensors on the rock surface and the SP reference electrode in the injection well) the pressure drop vs SP is plotted in Figure. 6, which shows excellent proportionality between the pressure drop and the SP response. The electrokinetic coupling coefficient is defined as the ratio of SP to pressure difference shown in Eq.3 (Jouniaux and Pozzi, 1995). At low injection pressures the variation of SP with pressure drop is linear, indicating a constant C_c. However for pressure drop higher than 850 psi, the magnitude of the C_c increases with pressure drop nonlinearly, which is shown in Figure 7. This increase of electrokinetic coupling coefficient is caused by the increased permeability at higher pore pressure due to dilatancy of microcracks and the related decrease in hydraulic tortuosity. The increase of zeta potential of new fracture surface areas also could contribute to the higher proportionality factor (Moore and Glaser, 2007). The difference in the chemical composition of the injection fluid and the pore fluid could also cause this behavior.

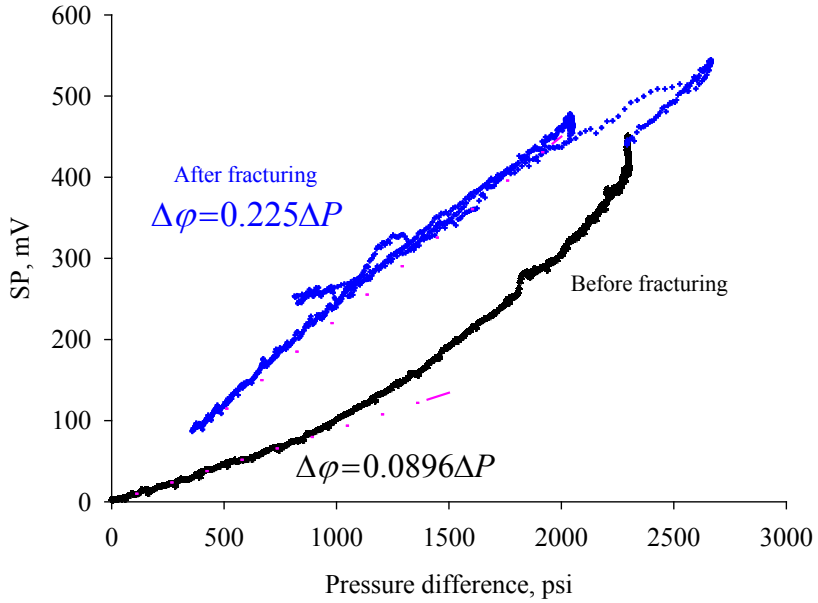

Figure 6. The electrokinetic coupling coefficient for different intervals (first cycle, data from SP sensor No. 6).

However, the injected fluid was from the same stock the rock was saturated in, so that chemical composition differences should have been small. As can be seen in Figure 7, there are small variations at low pressure drop values suggesting that chemical composition differences between the injected fluid and the pore fluid were indeed small. For the interval before fracturing, the electrokinetic coupling coefficient has a value is 0.0896 mV/psi for pressure drop less than 850 psi and its value is 0.2250mV/psi after fracturing (Figure. 6). After fracturing, the coefficient increased about 151%.

$$Cc = \frac{\Delta\varphi}{\Delta p} = \frac{\varepsilon\zeta}{\eta\sigma_f}\frac{F}{F_o} \tag{3}$$

where Cc, φ, p, ε, ζ, η, σ_f, F, F_o are electrokinetic coupling coefficient, electric potential, fluid pressure, absolute dielectric constant of the fluid, zeta potential, dynamic fluid viscosity, fluid conductivity, formation factor for the current sample conditions, and electrical formation factor respectively. Equation (3) is based on the assumption that the fluid flow is laminar, which requires low injection rate during the injection (Fitterman, 1978; Morgan, 1989).

During the first fracturing process, all production wells were closed and the pressures were recorded (Figure 8). It can be seen from the figure which production well is connected with the injection well by the fracture and which is not. In this case, no production well was connected by the induced fracture since the change of pressure in all the production wells show a large time delay compared with the change of pressure in the injection well and the pressure difference between the injection well and production wells are very large.

3.4 Test Parameters and Results of the Second Cycle of Fracturing Test

Since the fracture did not propagate to cross any of the production wells, a second fracturing stage was conducted to extend the facture to intersect some of the production wells. Figure. 9 shows the relevant data from the second fracturing period. The injection rate was set to 2.0 ml/min at the beginning and then was increased to 4.0 ml/min after the injection pressure slightly decreased (indicating reopening of the fracture induced during the first cycle). Then the injection rate was reduced by 99 percent after a pressure drop was detected. After 1 minute, the injection was resumed and it was ceased when a second pressure drop down was observed. Again, the test results show a correspondence between the pressure and the SP response. The first peak of pressure is about 2625 psi and the second peak is 2212 psi, both are lower than the break down pressure in the first fracturing test, which is expected since the fracture extended a little bit away from the injection well during the first fracturing. Figure 11 shows that for the pressure drop lower than 500 psi, the magnitude of C_c increased with pressure drop and this could be result from the slight chemi-

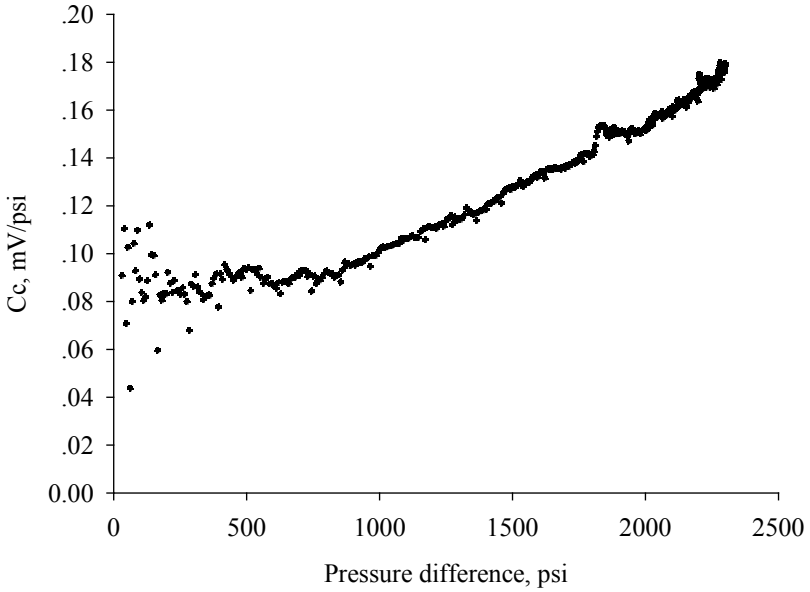

Figure 7. The variation of Cc with different pressure drop (first cycle, data from SP sensor No. 6).

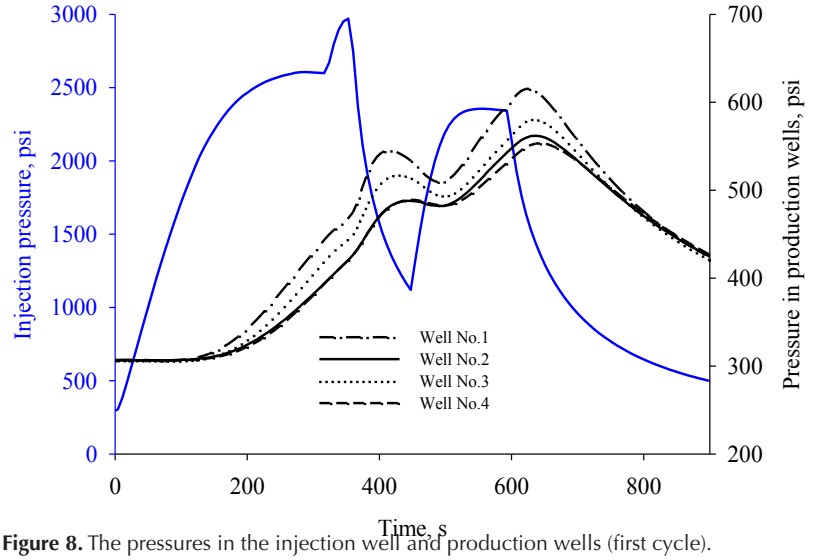

Figure 8. The pressures in the injection well and production wells (first cycle).

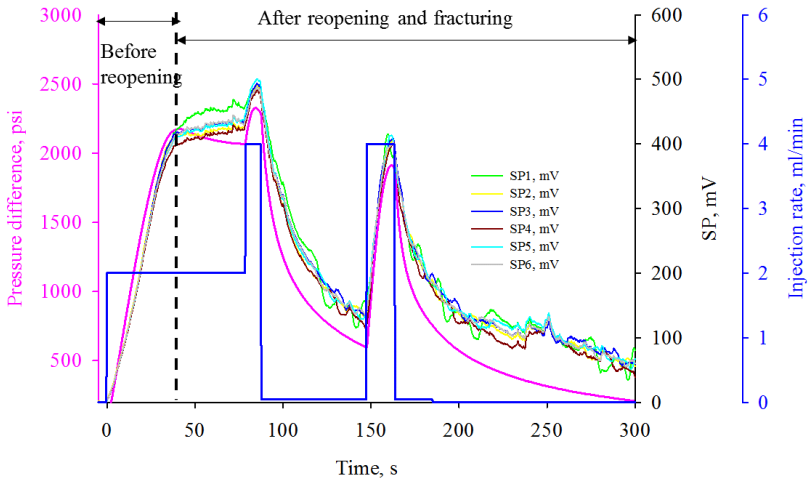

Figure 9. The recording data for second Sierra White granite block test (second cycle).

Figure 10. The electrokinetic coupling coefficient for different intervals (second cycle, data from SP sensor No. 6)

cal difference between the injection fluid and the fluid in the rock pores. At a higher pressure drop, the coupling coefficient almost remained at the same level. Then, for injection pressure higher than 850 psi, the magnitude of the C_c increased with pressure drop linearly. This increase of electrokinetic coupling coefficient is caused by the increased permeability at higher pore pressure due to dilatancy of microcracks and the related decreased hydraulic tortuosity. Increase of zeta potential of new fracture surface area also could contribute to the higher proportionality factor. The electrokinetic coupling coefficient for the second fracturing test is -0.118 mV/psi, and -0.216mV/psi before and after fracturing.

As before, the injection pressure and the pressures in the production wells were plotted and are shown in Figure. 12. It is obvious that the production well No.2 was interested by the induced fracture and the fracture did not reach to the rock surface. If it had, the pressure in the well would decline much faster considering that the pressure at the boundary was 300 psi.

3.5 Geometry of the Induced Fracture

After the test, the rock block was cut into slabs and the geometry of the induced fracture was reconstructed by compiling all the fracture traces on the slabs' surface. The reconstructed 3D fracture geometry does show that only one of the production well was connected by the induced fracture. During the entire hydraulic fracturing process, the recorded number of AE hits was less than expected. But, the observed localized AE events do provide a good indication regarding the geometry of the induced fracture as shown in Figure 13. The presence of water, squeezed AE sensor wires, poor coupling between the AE sensors, and electrical fields generated by other mechanisms resulted in a very high noise threshold.

3.6 Stepped Constant Pressure Experiment

After the successful hydraulic fracturing stage, a stepped constant pressure experiment was conducted to investigate the injection capacity of the block after fracturing. The stress condition was kept the same as the fracturing test. Also, the production wells were shut in during the test. To

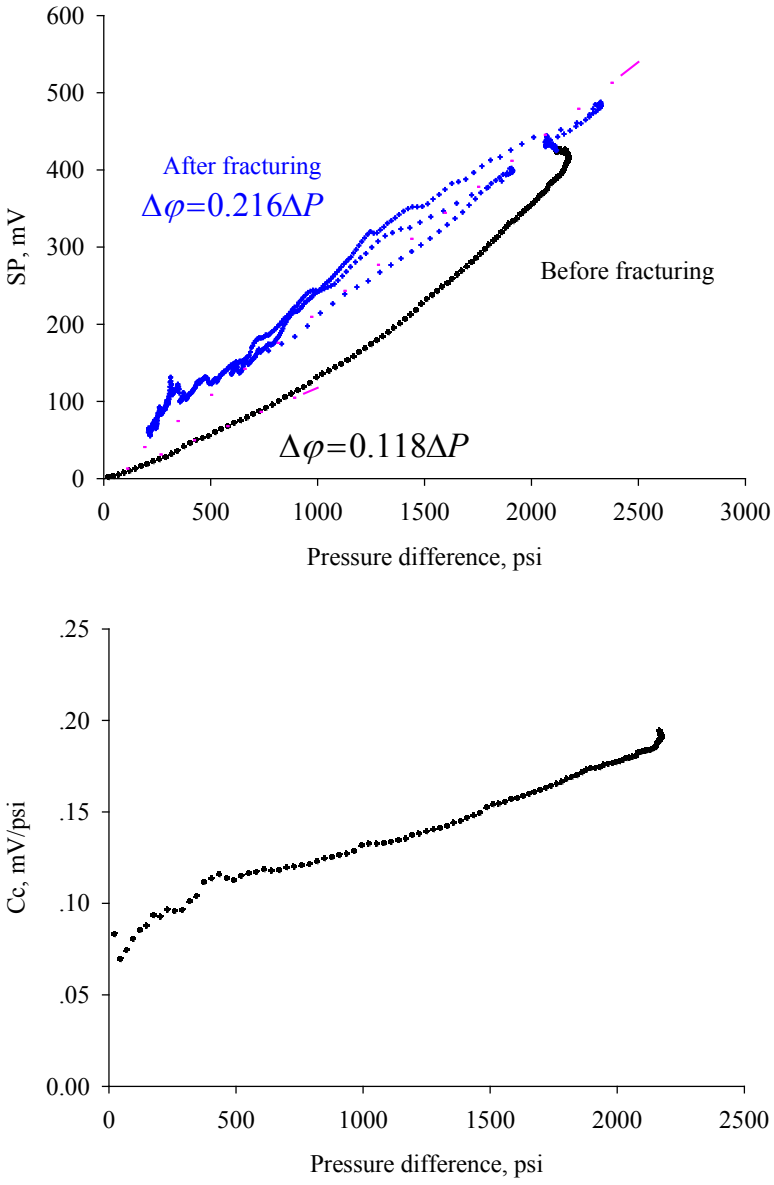

Figure 11. The variation of C_c with different pressure drop (first cycle, data from SP sensor No. 6)

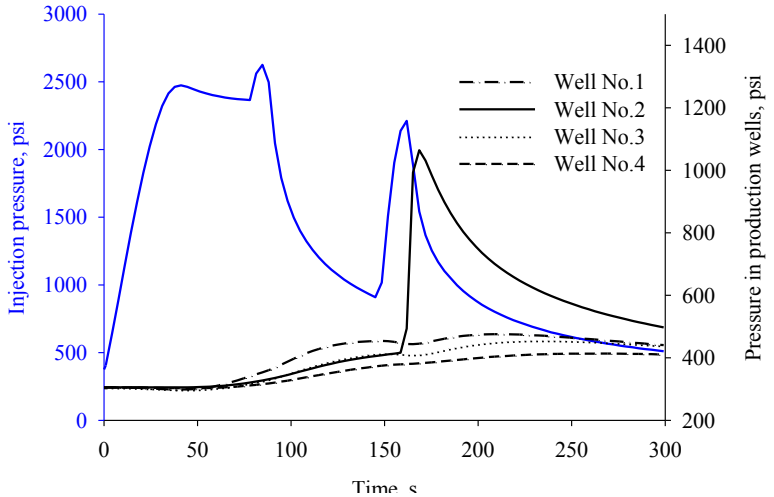

Figure 12. The pressures in the injection well and production wells (second block, first cycle).

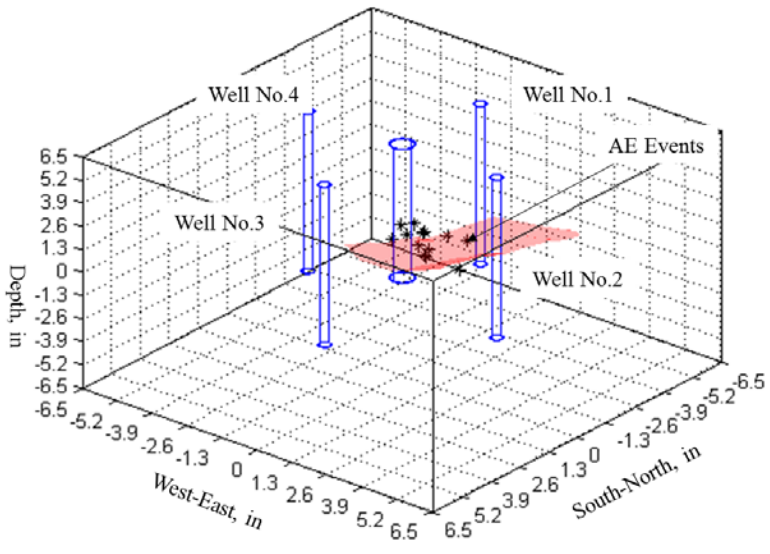

Figure 13. Geometry of the induced fracture interpreted from fluid flow behavior.

prevent further fracture propagation, the maximum injection pressure was set as 475 psi which is lower than the applied vertical in-situ stress. Figure 14 shows the injection pressure and fluid volume in the pump as a function of time. Figure.15 shows the injection rate under different injection pressures before and after stimulation. It is obvious that after stimulation the injection capacity of the block sample has increased dramatically and the injection rate increases linearly with pressure difference. According to Figure 15, after stimulation the injectivity of the block sample increased about 181% even with the induced fracture closed.

After one of the production wells was connected with the injection well by the induced fracture, we conducted a cold water circulation test in the heated block to investigate the heat and fluid exchange properties of the hydraulically induced fractures. Due to space limitations, data and analyse of the circulation experiment will be reported in the near future.

4. Summary and Conclusions

A new lab-scale polyaxial hydraulic fracturing test system has been developed. It allows EGS fracturing stimulation and fluid circulation to be simulated on laboratory scale. Hydraulic fracturing stimulation experiments along with elevated temperature circulation tests have been conducted. The results show an excellent relationship between SP response and the pressure drop during hydraulic fracturing. Also, a connection was made between the injection well and a production well by the hydraulic fracture, enabling circulation. The block stimulation resulted in injectivity increase of about 181%. The observed localized AE events are generally aligned with the trace of the induced fracture. The data from the circulation and tracer injection/production can shed light on the fracture surface area and analysis of flow/heat exchange properties of the hydraulically induced fracture. Work on these topics is ongoing and will be reported in the near future.

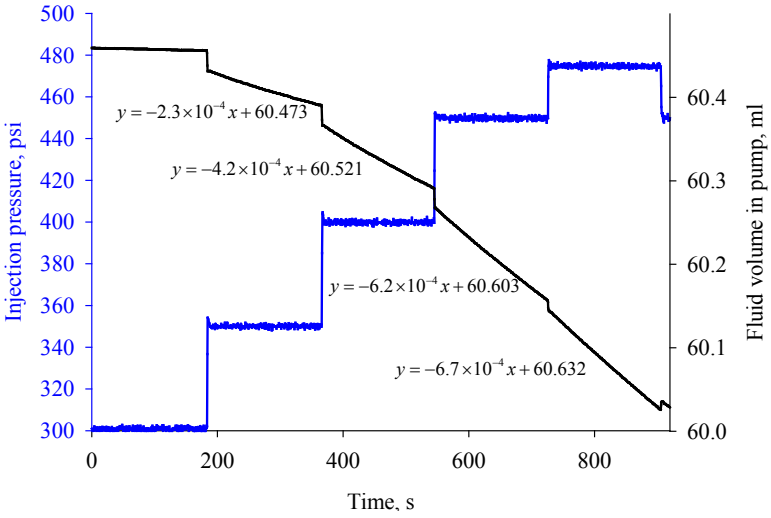

Figure 14. Stepped constant pressure experiment test after stimulation.

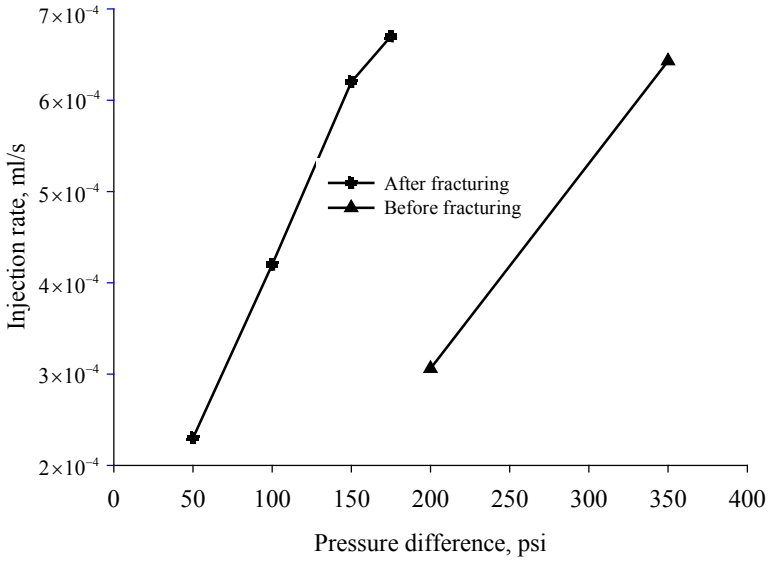

Figure 15. Injection rate of the rock sample before and after stimulation.

Acknowledgements

This project was supported by the U.S. Department of Energy Office of Energy Efficiency and Renewable Energy under Cooperative Agreement DE-EE0006765.0000. This support does not constitute an endorsement by the U.S. Department of Energy of the views expressed in this publica-

tion. The authors would like to thank two reviewers for their comments and suggestions that have improved the paper. We also thank Dr. T. Ishido for discussions and suggestions regarding SP measurement.

References

1. Fitterman D V. 1978. Electrokinetic and magnetic anomalies associated with dilatant regions in a layered earth. Journal of Geophysical Research: Solid Earth. 83(B12): 5923-5928.

2. Hu L, et al. 2016. Laboratory Scale Investigation of Enhanced Geothermal Reservoir Stimulation. Forty-first Workshop on Geothermal Reservoir Engineering, Stanford University, Stanford, California, February 22-24, 2016

3. Hubbert, M.K. and D.G. Willis. 1957. Mechanics of Hydraulic Fracturing. *Transactions of AIME*. 153-166.

4. Ishido, T., and J. W Pritchett. 2003. Characterization of fractured reservoirs using continuous self-potential measurements. In Proc. 28th Workshop on Geothermal Reservoir Engineering. 158-165.

5. Ishibashi T, et al. 2012. Experimental and Numerical Evaluation of Channeling Flow in Fractured Type of Geothermal Reservoir. Thirty-Seventh Workshop on Geothermal Reservoir Engineering, Stanford University, Stanford, California.

6. Jouniaux L, and Pozzi J P. 1995. Streaming potential and permeability of saturated sandstones under triaxial stress: Consequences for electrotelluric anomalies prior to earthquakes. *Journal of Geophysical Research: Solid Earth*. 100(B6): 10197-10209.

7. Moore, J.R., and Glaser, S.D. 2007. Self-potential observations during hydraulic fracturing. *Journal of Geophysical Research: Solid Earth*. 112.B2.

8. Morgan, F. D. 1989. Fundamentals of streaming potentials in geophysics: Laboratory methods. In Detection of subsurface flow phenomena. *Springer Berlin Heidelberg*. 133-144

9. MIT-Led Report. 2006. The Future of Geothermal Energy, ISBN: 0-615-13438-6.

10. Pritchett, J. W., and Ishido, T. 2005. Hydrofracture characterization using downhole electrical monitoring. *In Proceedings of World Geothermal Congress*, Turkey.

11. Yang Y, et al. 2012. Experimental study on fracture process of concrete by acoustic emission technology. *Przegląd Elektrotechniczny*. 88(9b): 55-58.